IEEE Access
Multidisciplinary | Rapid Review | Open Access Journal

Received June 12, 2019, accepted June 24, 2019, date of publication June 27, 2019, date of current version July 17, 2019.

Digital Object Identifier 10.1109/ACCESS.2019.2925370

Design of Vehicle Running States-Fused Estimation Strategy Using Kalman Filters and Tire Force Compensation Method

TE CHEN, (Student Member, IEEE), YINGFENG CAI, LONG CHEN, XING XU, (Member, IEEE), HAOBIN JIANG, AND XIAOQIANG SUN

School of Automotive and Traffic Engineering, Automotive Engineering Research Institute, Jiangsu University, Zhenjiang 212013, China

Corresponding authors: Long Chen (jsuchen123@foxmail.com) and Xing Xu (xuxing@mail.ujs.edu.cn)

This work was supported in part by the National Natural Science Foundation of China under Grant U1564201, Grant 51875255, and Grant U1664258, in part by the National Key Research and Development Program of China under Grant 2017YFB0102603, in part by the Six Talent Peaks Project of Jiangsu Province under Grant 2018-TD-GDZB-022, in part by the Primary Research and Development Plan of Jiangsu Province under Grant BE 2017129 and Grant BE2016149, and in part by the Postgraduate Scientific Research Innovation Program of Jiangsu Province under Grant SJKY19_2536.

ABSTRACT Accurate and reliable vehicle state estimation results are very significant to the active safety, energy optimization, and the intelligent control of vehicles. In this paper, to improve the accuracy and adaptability of vehicle running state estimation, the vehicle running states fused estimation strategy is presented for in-wheel motor drive electric vehicle using the Kalman filters and tire force compensation method. The concept of electric drive wheel model (EDWM) is developed and deduced, and then, considering that the EDWM is a nonlinear model with an unknown input, the design concept of high-order sliding mode observer is used to construct the state space equation of longitudinal force. To improve the accuracy and the reliability of vehicle state estimation, an overall estimation strategy with information fusion and tire force compensation is designed, in which a weighted square-root cubature Kalman filter with an adaptive covariance matrix of measurement noise is developed for observer design. Finally, the simulations in CarSim-Simulink co-simulation model and experiments are carried out, and the effectiveness of the designed estimation strategy is validated.

INDEX TERMS Electric vehicle, state estimation, information fusion, cubature Kalman filter.

I. INTRODUCTION

With the gradual increase of vehicle ownership, the environmental pollution problem caused by vehicle exhaust emissions is becoming more and more serious. The vigorous development of automobile industry and the rapid development of technology have promoted social change and progress [1], [2], but the related problems brought by it should not be ignored. With its zero-emission environmental protection characteristics, electric vehicles have become one of the recognized solutions to alleviate environmental pollution problem [3]–[5]. With the development and deepening of the research, a new drive type of electric vehicle, that is in-wheel motor drive electric vehicle, has attracted widespread attention [6], [7]. The in-wheel motor drive electric vehicle is actuated directly by the four in-wheel motors, which eliminates the complex transmission structure such as differential mechanism to make the mechanical structure more concise [8], [9]. Moreover, the four in-wheel motors can be independently controlled and have relatively high response speed, which greatly improves the degree of freedom in vehicle dynamics control, thus providing more design potential for vehicle energy optimization and stability control [10]–[12]. As we all know, in the closed-loop motion control system of vehicle, precise driving states of vehicles can provide reliable inputs for the control system, and is the basis for the good operation of the vehicle control system and achieving ideal control objectives [13]–[16]. However, some vehicle states need to be collected by extreme expensive sensors, and even some of them are difficult to be measured directly by vehicle-mounted sensors. In this case, people tend to design the model-based vehicle state observer [17], [18], using measurement information of

The associate editor coordinating the review of this manuscript and approving it for publication was Yue Cao.

 This work is licensed under a Creative Commons Attribution 3.0 License. For more information, see http://creativecommons.org/licenses/by/3.0/

low-cost sensor to calculate the required vehicle state variables, and apply it to the vehicle control system. Based on the above analysis, it is necessary and significant to pursue the research of vehicle state estimation [19]–[21].

In recent years, more and more advanced control theories have been introduced to the application research in the field of vehicle engineering [22]–[24]. Many researchers have achieved fruitful results in combination with the actual situation of vehicle dynamics [25], [26]. The Kalman filter is one of the most widely-used techniques in the studies of vehicle state estimation [27]–[30]. With the gradual improvement of consumer demand for vehicle performance, the precision degree of vehicle is getting higher and higher, and the vehicle control system is becoming more and more complex correspondingly, which cause that the current vehicles are dependent on more accurate vehicle state estimation results [31]–[35]. In this case, a series of improved Kalman filter methods have been widely studied and applied, in which the effect of estimation has been significantly improved [36]–[41]. In [42], the vehicle dynamics model has been established with the longitudinal, lateral, and vertical kinetic equations being considered, to obtain the estimation of vehicle sideslip angle, the extended Kalman filter and the recursive least squares algorithm is combined to design the observer and improve the estimation accuracy. In [43], the full-state vehicle dynamics model and modified tire model are considered, and the unscented Kalman filter is designed with estimation fusion method, in which the interacting multiple model method is applied to adjust the weights of different nonlinear models. In addition, some researchers also pay attention to the influence of uncertainties such as non-linear disturbances on estimation results, and many novel estimation strategies have been designed [44]–[48]. With the revolution of sensor technology and the improvement of sensor production capacity, some researchers have adopted new sensors or low-cost sensors to design different and novel estimation strategies, and created some new ideas for observer design [49]–[53]. The cubature Kalman filter method avoids the complex calculation of Jacobian matrix and the problem of excessive large error or even divergence of the filter caused by the system nonlinearity in extended Kalman filter. Moreover, the cubature Kalman filter can effectively avoid the problem of high-dimensional stability degradation of existed in unscented Kalman filter. Among the existing Kalman filter algorithms, the cubature Kalman filter is the most accurate filtering algorithm in theory, which can provide a reliable theoretical basis for vehicle driving state estimation. In addition, in the design process of vehicle driving state estimation strategy, if we can make full use of the existing redundant state information, through information compensation and iteration, it will help to further improve the overall estimation accuracy.

In this paper, motivated by above analysis, a design of vehicle running states fused estimation strategy using Kalman filters and tire force compensation method is proposed. Utilizing the electric-driving characteristics of in-wheel motor drive electric vehicle, the concept of electric drive wheel model (EDWM) is developed and deduced. The vehicle model with 3 degree of freedom, the EDWM, and the tire model are established for observer design. A weighted square-root cubature Kalman filter (WCKF) is studied for vehicle state estimation with the covariance matrix of measurement noise being adjusted in real time. Considering that the EDWM is a nonlinear model with unknown input, to facilitate the estimation of longitudinal tire force, the design concept of high-order sliding mode observer is used to construct the state space equation of longitudinal force. Then, the multi-dimensional state space discrete model is presented for the vehicle state estimation based on the WCKF. In order to improve the accuracy and reliability of the estimation system, an overall estimation strategy with information fusion and tire force compensation is designed, in which the longitudinal and lateral tire force can be compensated adaptively and the redundancy of information is fully utilized to improve the accuracy and adaptability of estimation results.

The rest of this paper is organized as follows. The vehicle model is presented in Section 2. The fused method for vehicle running state estimation based on Kalman filter is designed in Section 3. The simulation results are shown in Section 4. The experimental verification is shown in Section 5, followed by the conclusive remarks.

II. VEHICLE MODEL

A. VEHICLE DYNAMIC MODEL

A schematic diagram of vehicle model with 3 degree of freedom (3-DOF) in the longitudinal, lateral, and yaw directions is shown in Fig. 1. The origin of dynamic coordinate system xoy fixed on the vehicle coincides with the vehicle gravity center, in which the x axis is the longitudinal axis of the vehicle (the forward direction is positive), and the y axis is the lateral axis of the vehicle (the right-to-left direction is positive). The pitch, roll, vertical motions and the suspension system of the vehicle are ignored. It is assumed that the mechanical properties of each tire are the same. The serial numbers 1, 2, 3, and 4 of four wheels are respectively corresponding to the front-left, the front-right, the rear-left and

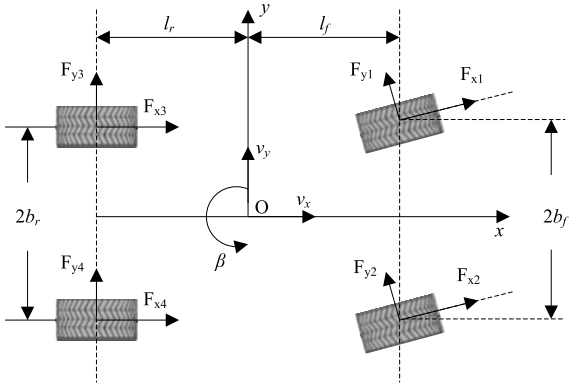

FIGURE 1. Vehicle dynamics model.

the rear-right wheel. The dynamic equations of the 3-DOF vehicle model can be expressed as

$$\dot{v}_x = \gamma v_y + a_x \tag{1}$$

$$\dot{v}_y = -\gamma v_x + a_y \tag{2}$$

$$\begin{aligned} I_z\dot{\gamma} = {} & (F_{x1} + F_{x2})\, l_f \sin\delta - (F_{y3} + F_{y4}) l_r \\ & + \left(F_{y1} + F_{y2}\right) l_f \cos\delta + (F_{y1} - F_{y2}) b_f \sin\delta \\ & - (F_{x1} - F_{x2}) b_f \cos\delta - (F_{x3} - F_{x4}) b_r \end{aligned} \tag{3}$$

where v_x and v_y represents the longitudinal and lateral vehicle speed, respectively. And a_x and a_y represents the longitudinal and lateral vehicle acceleration, respectively. γ represents the yaw rate, m is the vehicle mass, δ represents the steering angle of the front wheels, I_z stands for the moment of inertia. F_{xj} and $F_{yj}(j = 1, 2, 3, 4)$ are the longitudinal and lateral forces of the jth tire, respectively. l_f and l_r are the distances from vehicle gravity center to the front and rear axle, respectively. b_f and b_r are the half treads of the front wheels and rear wheels, respectively. The longitudinal and lateral vehicle acceleration are computed as

$$a_x = \frac{1}{m}(F_{x1} + F_{x2})\cos\delta - \left(F_{y1} + F_{y2}\right)\sin\delta + F_{x3} + F_{x4} \tag{4}$$

$$a_y = \frac{1}{m}(F_{x1} + F_{x2})\sin\delta + \left(F_{y1} + F_{y2}\right)\cos\delta + F_{y3} + F_{y4} \tag{5}$$

The vehicle sideslip angle can be expressed as

$$\beta = v_y / v_x \tag{6}$$

where β represents the vehicle sideslip angle.

B. DEDUCTION OF EDWM

The diagrammatic sketch of EDWM is shown in Fig. 2. The in-wheel motor drive electric vehicle studied in this paper is actuated by four in-wheel motors, and the electromechanical coupling driving wheel composed of a motor and a tire can be considered as an independent information module, so the concept of the EDMW is introduced to the longitudinal force estimation process and the current, speed and voltage are used to estimate the longitudinal force. The rotational dynamic equation of EDWM is expressed as

$$J_1\dot{\omega}_j = T_{Lj} - F_{xj} r \tag{7}$$

where ω_j represents the rotational speed of the jth wheel, J_1 denotes the inertia moment, r represents the effective rolling radius of EDWM, T_{Lj} stands for the load torque of in-wheel motor. The balance equation of torque in the output shaft of EDWM is shown as

$$J_2\dot{\omega}_j + b\omega_j = K_t i_j - T_{Lj} \tag{8}$$

where J_2 is the rotational inertia of in-wheel motor rotor, b is the damping coefficient, K_t is the motor torque constant, i_j is the bus current. The dynamic voltage balance equation of equivalent circuit in-wheel motor can be modeled as

$$U_j = Ri_j + Li_j + K_a\omega_j \tag{9}$$

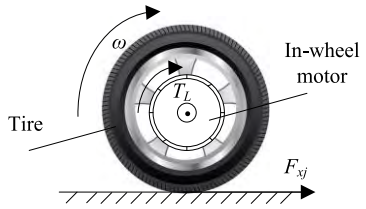

FIGURE 2. Electric driving wheel model.

where U_j is the bus voltage of in-wheel motor, R is the equivalent resistance of winding, L is the equivalent inductance of winding, K_a is the inverse electromotive force coefficient. Substituting equation (7) into equation (8) and combining it with equation (9), we can obtain the EDWM as follows,

$$\dot{i}_j = -\frac{R}{L} i_j - \frac{K_a}{L}\omega_j + \frac{1}{L}U_j \tag{10}$$

$$\dot{\omega}_j = \frac{K_t}{J} i_j - \frac{b}{J}\omega_j - \frac{r}{J}F_{xj} \tag{11}$$

where $J = J_1 + J_2$.

C. TIRE MODEL

The empirical magic formula of tire model is used in order to estimate the longitudinal and lateral tire forces, which can be computed as

$$F_y = D\sin\{C\arctan[B\alpha - E(B\alpha - \arctan(B\alpha))]\} \tag{12}$$

where B is the stiffness factor, C is the curve shape factor, D is the peak factor, E is the curve curvature factor, α is the wheel side slip angle. The tire model parameters like B, C, D, E, are related to the tire vertical load. The vertical load of each tire can be calculated as

$$\begin{cases} F_{z1} = l_r\left(\dfrac{mg}{2l} + \dfrac{ma_y h}{2b_f l}\right) - \dfrac{ma_x h}{2l} \\ F_{z2} = l_r\left(\dfrac{mg}{2l} - \dfrac{ma_y h}{2b_f l}\right) - \dfrac{ma_x h}{2l} \\ F_{z3} = l_f\left(\dfrac{mg}{2} + \dfrac{ma_y h}{2b_r l}\right) + \dfrac{ma_x h}{2l} \\ F_{z4} = l_f\left(\dfrac{mg}{2} - \dfrac{ma_y h}{2b_r l}\right) + \dfrac{ma_x h}{2l} \end{cases} \tag{13}$$

where F_{z1}, F_{z2}, F_{z3}, and F_{z4} are the vertical load of corresponding tires, h is the height of the center of gravity, g is the acceleration of gravity. The side slip angle of each wheel can be obtained by

$$\begin{cases} \alpha_1 = \delta - \arctan\dfrac{v_y + l_f\gamma}{v_x + b_f\gamma/2} \\ \alpha_2 = \delta - \arctan\dfrac{v_y + l_f\gamma}{v_x - b_f\gamma/2} \\ \alpha_3 = -\arctan\dfrac{v_y - l_r\gamma}{v_x + b_r\gamma/2} \\ \alpha_4 = -\arctan\dfrac{v_y - l_r\gamma}{v_x - b_r\gamma/2} \end{cases} \tag{14}$$

The tire slip rate can be obtained as

$$s_j = \mathrm{sgn}\left(\omega_j r - v_{rj}\right) \frac{\max\left(v_{\pi j}, \omega_j r\right) - \min\left(v_{rj}, \omega_j r\right)}{\max\left(v_{nj}, \omega_j r\right)} \tag{15}$$

where s_j represents the tire slip rate of jth tire, n_j represents the wheel rotating speed of jth tire, v_{nj} represents the wheel linear velocity of jth tire, r represents the effective wheel radius. The coupling relationship of four-wheel speed can be expressed as

$$\begin{cases} \omega_1 = \dfrac{30}{\pi r}\left[\left(v_x + b_f\gamma\right)\cos\delta + \left(v_y + l_f\gamma\right)\sin\delta\right] \\ \omega_2 = \dfrac{30}{\pi r}\left[\left(v_x - b_f\gamma\right)\cos\delta + \left(v_y + l_f\gamma\right)\sin\delta\right] \\ \omega_3 = \dfrac{30}{\pi r}\left(v_x + b_r\gamma\right) \\ \omega_4 = \dfrac{30}{\pi r}\left(v_x - b_r\gamma\right) \end{cases} \tag{16}$$

III. FUSED MEHTOD FOR VEHICLE RUNNING STATE ESTIMATION METHOD BASED ON KALMAN FILTERS

A. WEIGHTED SQUARE-ROOT CUBATURE KALMAN FILTER (WCKF)

The vehicle dynamics model can be expressed as the following discrete state space equations

$$\begin{aligned} x_k &= f\left(x_{k-1}\right) + w_{k-1} \\ y_k &= h\left(x_k\right) + v_k \end{aligned} \tag{17}$$

where x_k is the state vector of system, y_k is the measurement vector of system. $f(\bullet)$ and $h(\bullet)$ are the nonlinear functions and represents the state transition matrix of state equation and measurement equation, respectively. w_k and v_k represents the system noise and measurement noise, respectively, and they are the uncorrelated white noise vectors of zero mean. The covariance matrix of w_k and v_k is Q_k and R_k, respectively.

In order to guarantee the symmetry and non-negative definiteness of covariance matrix, and improve the estimation accuracy of cubature Kalman filter, in the existing state estimation researches, the square-root cubature Kalman filter is widely used, in which the square root form of the error covariance matrix is used for iteration. The square-root cubature Kalman filter requires precise prior statistical information of measurement noise. When the statistical characteristics of measurement noise are uncertain, the filtering accuracy will decrease or even diverge. For the estimation of vehicle driving state, the factors such as complex driving environment, various state changes and uncertainties will cause the change of statistical characteristics of measurement noise. The covariance matrix of measurement noise is adjusted online by using the moving window estimation method, and the idea of weighting is introduced. According to the usefulness of information at different time for measurement noise statistics, the weights of information at different time in the window are dynamically adjusted to enhance the utilization of useful information, which can effectively improve the estimation accuracy of vehicle state filtering. The iteration steps of weighted square-root cubature Kalman filter can be written as

(S1) Initialization:

The initial state value and the initial mean square root of error covariance matrix can be expressed as

$$\begin{aligned} \hat{x}_0 &= E\left(x_0\right) \\ S_0 &= \sqrt{E\left(\left(x_0 - \hat{x}_0\right)\left(x_0 - \hat{x}_0\right)^T\right)} \end{aligned} \tag{18}$$

where $\hat{x}_0$ denotes the initial state value, S_0 is the initial mean square root of error covariance matrix.

(S2) Computation of cubature points:

The third-order spherical-radial volume criterion is used to calculate sampling points and weights.

$$x_{i,k-1/k-1} = S_{k-1/k-1}\xi_i + \hat{x}_{k-1/k-1}, \quad i = 1, 2, \cdots, 2n \tag{19}$$

where i are the serial numbers of cubage points, $S_{k-1/k-1}$ is the square root of error covariance matrix $P_{k-1/k-1}$ and can be computed as $P_{k-1/k-1} = S_{k-1/k-1}S_{k-1/k-1}^T$, ξ_i can be written as

$$\begin{aligned} \xi_i &= x_{k-1} + \sqrt{nP_x}e_i \\ w_i &= \frac{1}{n}, \quad i = 1, 2, \cdots, 2n \end{aligned} \tag{20}$$

where e_i is ith unit vector with element 1, w_i is the weight.

(S3) Time update:

Firstly, the cubature point propagation is carried out.

$$\begin{aligned} x_{k/k-1}^* &= \sqrt{w_1}\left(x_{1,k/k-1} - \hat{x}_{k/k-1}\right) \\ &\quad \cdots \sqrt{w_{2n}}\left(x_{2n,k/k-1} - \hat{x}_{k/k-1}\right) \\ x_{i,k/k-1} &= f\left(\xi_{i,k-1}\right), \quad i = 1, 2, \cdots, 2n \end{aligned} \tag{21}$$

Then, calculate the one-step prediction state.

$$\begin{aligned} \hat{x}_{k/k-1} &= \sum_{i=1}^{2n} w_i x_{i,k/k-1} \\ S_{k/k-1}^T &= QR\left[\left(x_{k/k-1}^* S_{Q,k-1}\right)^T\right] \end{aligned} \tag{22}$$

where QR represents the orthogonal-triangular decomposition, $S_{Q,k-1}$ is the square root of system noise error covariance matrix.

(S4) Measurement update:

The innovation vector is expressed as

$$\varepsilon_k = y_k - h\left(\hat{x}_{k/k-1}\right) \tag{23}$$

The optimal estimation of covariance matrix of innovation vector in sliding sampling interval with length N is obtained by moving window method.

$$\hat{R}_k = \sum_{j=1}^{N} \varepsilon_{k-j}\varepsilon_{k-j}^T \tag{24}$$

$$\hat{R}_k = \frac{1}{N}\left(\sum_{j=1}^{N}\varepsilon_{k-j}\varepsilon_{k-j}^T - \sum_{i=1}^{2n} w_i\left(h\left(\varepsilon_{i,\text{k-j}/k-j-1}\right) - \hat{y}_{k-j/k-j-1}\varepsilon_{k-j}^T\right)\left(h\left(\varepsilon_{i,\text{k-j}/k-j-1}\right) - \hat{y}_{k-j/k-j-1}\varepsilon_{k-j}^T\right)^T\right) \tag{25}$$

where $\hat{R}_k$ is the covariance matrix of innovation vector. The moving window method can calculate the approximate statistical characteristics of measurement noise at the current time by using the information in the window range, and can realize the online estimation of measurement noise statistics. However, it is unable to accurately get the real situation of current measurement noise statistics by using the same weights for each time in the window without distinguishing them. Therefore, a weighted method is used to set different weights according to the usefulness of information at different times in the window, which makes the estimated statistical characteristics of measurement noise more accurate. The covariance matrix of weighted innovation vector is written as (25), shown at the top of this page, where N is the length of moving window.

The Cholesky factorization is obtained as

$$\begin{aligned} S_{yy,k/k-1}^T &= QR\left[\left(y_{k/k-1}\,\text{Chol}\left(\hat{R}_k\right)\right)^T\right] \\ P_{xz,k/k-1} &= x'_{k/k-1}y_{k/k-1}^T \end{aligned} \tag{26}$$

where *Chol* represents the Cholesky decomposition. In formula (25), the moving window length can be expressed as $\frac{1}{N}$=c$_i$ $= \sqrt{\varepsilon_{k-j}\varepsilon_{k-j}^T}$, where c_i is the weight coefficient. That is, the size of weight coefficient will change with the variation of the iteration error, and by Cholesky decomposition, the obtained covariance matrix of innovation vector will vary with the statistical characteristics of iteration error at the current sampling time. The cubature points used for measurement update is calculated as

$$\begin{aligned} x'_{k/k-1} = &\sqrt{w_1}\left(\xi_{1,k/k-1} - \hat{y}_{k/k-1}\right) \\ &\cdots\sqrt{w_{2n}}\left(\xi_{2n,k/k-1} - \hat{y}_{k/k-1}\right) \end{aligned} \tag{27}$$

where $\hat{y}_{k/k-1} = \sum_{i=1}^{2n} w_i h\left(\xi_{i,k/k-1}\right)$. The propagation of cubature point is expressed as $y_{i,k/k-1} = h\left(x_{i,k/k-1}\right)$, then, the prediction results of measurements can be expressed as

$$\begin{aligned} y_{k/k-1} = &\sqrt{w_1}\left(h\left(\xi_{1,k/k-1}\right) - \hat{y}_{k/k-1}\right) \\ &\cdots\sqrt{w_{2n}}\left(h\left(\xi_{2n,k/k-1}\right) - \hat{y}_{k/k-1}\right) \end{aligned} \tag{28}$$

The state update equation is

$$\hat{x}_k = \hat{x}_{k/k-1} + G_k\left(y_k - \hat{y}_{k/k-1}\right) \tag{29}$$

where $G_k = P_{xy,k/k-1}P_{yy,k/k-1}^{-1} = \left(P_{xy,k/k-1}/P_{yy,k/k-1}^T\right)/P_{yy,k/k-1}^T$, $S_k^T = QR\left[\left(x'_{k/k-1} - G_k y_{k/k-1} G_k S_{R,k}\right)^T\right]$.

B. VEHICLE RUNNING STATE PRELIMINARY ESTIMATION USING WCKF

In order to obtain the preliminary estimation results of vehicle driving state, the discretization results of equation (1), (2), (3), (9), (10) can be expressed as $x_{1,k}$, shown at the bottom of the next page,

$$\begin{aligned} x_{1,k} &= f_1\left(x_{k-1}\right) + w_{k-1} \\ y_{1,k} &= h_1\left(x_k\right) + v_k \end{aligned} \tag{30}$$

As we can see in the system state vector of equation (30), in order to facilitate the design of longitudinal tire force estimation method, the derivative of longitudinal tire force is introduced into the system state vector. Integrating the design method of high-order sliding mode observer, the state equation of longitudinal tire force is written as

$$\begin{aligned} &\begin{bmatrix}\dot{x}_{1,12-15}\\ \dot{x}_{1,16-19}\end{bmatrix} = \begin{bmatrix}\dot{F}_{xj}\\ \ddot{F}_{xj}\end{bmatrix} \\ &= \begin{bmatrix}\dot{F}_{xj}\\ -k_1\,\text{sgn}\left(\dot{F}_{xj} - F_{xj}\right) - k_2\left(\dot{F}_{xj} - F_{xj}\right)\end{bmatrix} \\ &= \begin{bmatrix}x_{1,16-19}\\ -k_1\,\text{sgn}\left(x_{1,16-19} - x_{1,12-15}\right) - k_2\left(x_{1,16-19} - x_{1,12-15}\right)\end{bmatrix} \end{aligned} \tag{31}$$

where k_1 and k_2 are the sliding mode observer parameters. Then, the discrete state transition equation can be expressed as (32), shown at the bottom of the next page, where T represents the sampling period of the Kalman filter. As we can see in formula (32), the sliding-mode-observer-based state equations are introduce into the Kalman filter, and this integrated observer design method can effectively suppress chattering phenomena via the update and iteration of Kalman filter. The designed observer in this section is marked as WCKF-A. In the design of WCKF-A, the current, speed, and voltage of EDWM measured by vehicular sensors, the steering angle of front wheel, the longitudinal and lateral acceleration of vehicle, the yaw rate, and the lateral tire forces, are used as the known inputs of WCKF-A. With the presented WCKF-A, the vehicle running state can be estimated.

C. OVERALL ESTIMATION STRATEGY WITH INFORMATION FUSION AND TIRE FORCE COMPENSATION

As we can see in WCKF-A, the estimation results of longitudinal tire force depend on vehicle longitudinal force dynamics performance more obviously. When the vehicle tire slips longitudinally, the estimated results of the observer are likely to be affected to some extent. In order to obtain more accurate and reliable estimation results, a novel overall estimation strategy with information fusion and tire force compensation is proposed, as shown in Fig. 3. The subscript A in the symbol

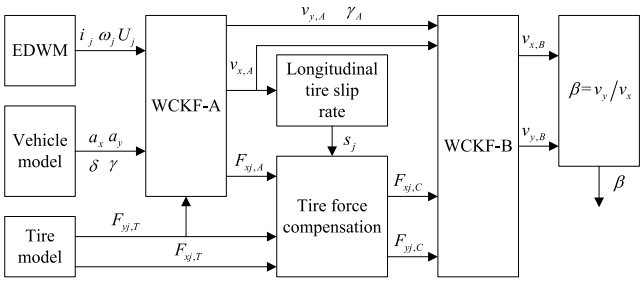

FIGURE 3. Overall estimation strategy.

of vehicle state estimation results represents the estimation results of WCKF-A, the subscript B in the symbol of vehicle state estimation results represents the estimation results of WCKF-B, the subscript C represents the compensation results of tire forces, the subscript T represents the output results of tire model.

In order to suppress the influence of longitudinal tire slip on the calculation results of longitudinal force, the longitudinal tire slip rate is used to compensation the estimation results of WCKF-A. The longitudinal tire slip rate is obtained by equation (15), then, the compensation result of longitudinal tire can be designed as

$$F_{xj,C} = \left(\frac{1}{2} + 2^{-\frac{1}{|s_j|}}\right) F_{xj,T} + \left(\frac{1}{2} - 2^{-\frac{1}{|s_j|}}\right) F_{xj,A} \quad (33)$$

In WCKF-A, the longitudinal tire forces are obtained by longitudinal dynamics relations and vehicle-mounted current, speed and voltage sensors. Therefore, the estimation results

where $x_{1,k} = \begin{bmatrix} x_{1,1} & x_{1,2} & x_{1,3} & x_{1,4} & x_{1,5} & x_{1,6} & x_{1,7} & x_{1,8} & x_{1,9} & x_{1,10} x_{1,11} & x_{1,12} & x_{1,13} & x_{1,14} & x_{1,15} & x_{1,16} & x_{1,17} & x_{1,18} & x_{1,19} \end{bmatrix}^T$

$= \begin{bmatrix} v_{x,k} & v_{y,k} & \gamma_k & i_{1,k} & i_{2,k} & i_{3,k} & i_{4,k} \omega_{1,k} & \omega_{2,k} & \omega_{3,k} & \omega_{4,k} & F_{x1,k} & F_{x2,k} & F_{x3,k} & F_{x4,k} & \dot{F}_{x1,k} & \dot{F}_{x2,k} & \dot{F}_{x3,k} & \dot{F}_{x4,k} \end{bmatrix}^T$

$y_{1,k} = \begin{bmatrix} y_{1,1} & y_{1,2} & y_{1,3} & y_{1,4} & y_{1,5} & y_{1,6} & y_{1,7} & y_{1,8} & y_{1,9} \end{bmatrix}^T = \begin{bmatrix} \gamma_k & i_{1,k} & i_{2,k} & i_{3,k} & i_{4,k} & \omega_{1,k} & \omega_{2,k} & \omega_{3,k} & \omega_{4,k} \end{bmatrix}^T$

$$\begin{bmatrix} x_{1,1,k} \\ x_{1,2,k} \\ x_{1,3,k} \\ x_{1,4,k} \\ x_{1,5,k} \\ x_{1,5,k} \\ x_{1,7,k} \\ x_{1,8,k} \\ x_{1,9,k} \\ x_{1,10,k} \\ x_{1,12,k} \\ x_{1,13,k} \\ x_{1,14,k} \\ x_{1,15,k} \\ x_{1,16,k} \\ x_{1,17,k} \\ x_{1,18,k} \\ x_{1,19,k} \end{bmatrix} = \begin{bmatrix} x_{1,1,k-1} + \left(x_{1,3,k-1} x_{1,2,k-1} + a_{x,k-1}\right) \cdot T \\ x_{1,2,k-1} + \left(-x_{1,3,k-1} x_{1,1,k-1} + a_{y,k-1}\right) \cdot T \\ x_{1,3,k-1} + \frac{1}{I_z} \left[\left(x_{1,12,k-1} + x_{1,13,k-1}\right) l_f \sin\delta_{k-1} - \left(F_{y3,k-1} + F_{y4,k-1}\right) l_r + \left(F_{y1,k-1} + F_{y2,k-1}\right) l_f \cos\delta_{k-1} \right. \\ \left. + \left(F_{y1,k-1} - F_{y2,k-1}\right) b_f \sin\delta_{k-1} - \left(x_{1,12,k-1} - x_{1,13,k-1}\right) b_f \cos\delta_{k-1} - \left(x_{1,14,k-1} - x_{1,15,k-1}\right) b_r \right] \cdot T \\ x_{1,4,k-1} + \left(-\frac{R}{L} x_{1,4,k-1} - \frac{K_a}{L} x_{1,8,k-1} + \frac{1}{L} U_{1,k-1}\right) \cdot T \\ x_{1,5,k-1} + \left(-\frac{R}{L} x_{1,5,k-1} - \frac{K_a}{L} x_{1,9,k-1} + \frac{1}{L} U_{2,k-1}\right) \cdot T \\ x_{1,6,k-1} + \left(-\frac{R}{L} x_{1,6,k-1} - \frac{K_a}{L} x_{1,10,k-1} + \frac{1}{L} U_{3,k-1}\right) \cdot T \\ x_{1,7,k-1} + \left(-\frac{R}{L} x_{1,7,k-1} - \frac{K_a}{L} x_{1,11,k-1} + \frac{1}{L} U_{4,k-1}\right) \cdot T \\ x_{1,8,k-1} + \left(\frac{K_t}{J} x_{1,4,k-1} - \frac{b}{J} x_{1,8,k-1} - \frac{r}{J} x_{1,12,k-1}\right) \cdot T \\ x_{1,9,k-1} + \left(\frac{K_t}{J} x_{1,5,k-1} - \frac{b}{J} x_{1,9,k-1} - \frac{r}{J} x_{1,13,k-1}\right) \cdot T \\ x_{1,10,k-1} + \left(\frac{K_t}{J} x_{1,6,k-1} - \frac{b}{J} x_{1,10,k-1} - \frac{r}{J} x_{1,14,k-1}\right) \cdot T \\ x_{1,11,k-1} + \left(\frac{K_t}{J} x_{1,7,k-1} - \frac{b}{J} x_{1,11,k-1} - \frac{r}{J} x_{1,15,k-1}\right) \cdot T \\ x_{1,12,k-1} + x_{1,16,k-1} \cdot T \\ x_{1,13,k-1} + x_{1,17,k-1} \cdot T \\ x_{1,14,k-1} + x_{1,18,k-1} \cdot T \\ x_{1,15,k-1} + x_{1,19,k-1} \cdot T \\ x_{1,16,k-1} + \left(-k_1 \operatorname{sgn}\left(x_{1,16,k-1} - x_{1,12,k-1}\right) - k_2 \left(x_{1,16,k-1} - x_{1,12,k-1}\right)\right) \cdot T \\ x_{1,17,k-1} + \left(-k_1 \operatorname{sgn}\left(x_{1,17,k-1} - x_{1,13,k-1}\right) - k_2 \left(x_{1,17,k-1} - x_{1,13,k-1}\right)\right) \cdot T \\ x_{1,18,k-1} + \left(-k_1 \operatorname{sgn}\left(x_{1,18,k-1} - x_{1,1,k-1}\right) - k_2 \left(x_{1,19,k-1} - x_{1,14,k-1}\right)\right) \cdot T \\ x_{1,19,k-1} + \left(-k_1 \operatorname{sgn}\left(x_{1,19,k-1} - x_{1,15,k-1}\right) - k_2 \left(x_{1,19,k-1} - x_{1,15,k-1}\right)\right) \cdot T \end{bmatrix} \quad (32)$$

of WCKF-A have the advantage of fast information acquisition. The computation results of tire model are stable and accurate, and are not easily affected by the driving state of vehicle. However, the calculation of tire model is relatively large. When the vehicle driving state changes dramatically, the calculation speed is relatively slow, and the calculation results may also have a certain lag. As we can see in equation (33), the presented compensation method can effectively combine the advantages of these two methods. When the longitudinal tire slip rate is large, the weight of tire model calculation results is increased, and the weight of WCKF-A is reduced. Similarly, when the longitudinal tire slip rate is small, the weight of tire model calculation results is reduced, and the weight of WCKF-A is increased. Thus, the designed compensation method can adjust tire force estimation results adaptively according to vehicle driving conditions. Based on equation (33), the lateral tire force compensation method can be designed as

$$F_{yj,C} = F_{yj,T} + k_p \left(F_{xj,C} - F_{xj,T}\right) + k_i \int \left(F_{xj,C} - F_{xj,T}\right) s_j dt \tag{34}$$

where k_p and k_i represents the proportional parameter and integral parameter, respectively.

As shown in Fig. 3, the compensation results of tire forces, and the estimated vehicle running states by WCKF-A are used as the known inputs of WCKF-B to obtain more reliable vehicle state estimation results by fusing the known data according to the redundancy of information. In the design of WCKF-B, according to the equation (1), (2), (3), (4), (4), the discretization results of equation can be expressed as

$$\begin{aligned} x_{2,k} &= f_2\left(x_{k-1}\right) + w_{k-1} \\ y_{2,k} &= h_2\left(x_k\right) + v_k \end{aligned} \tag{35}$$

where $x_{2,k} = \left[x_{2,1,k}\ x_{2,2,k}\ x_{2,3,k}\right]^T = \left[v_{x,k}\ v_{y,k}\ \gamma_k\right]^T$, $y_{2,k} = \left[y_{2,1,k}\ y_{2,2,k}\ y_{2,3,k}\right]^T = \left[\gamma_k\ a_{x,k}\ a_{y,k}\right]^T$. The discrete state transition equation of WCKF-B is written as (36), shown at the bottom of this page. In WCKF-B, the longitudinal vehicle speed, lateral vehicle speed and yaw rate estimated by WCKF-A, and the tire force compensation results are used as the inputs of WCKF-B. According to the estimation results of WCKF-B, the vehicle sideslip angle can be obtained by equation (6).

IV. SIMULATION RESULTS

In order to verify the effectiveness of the proposed estimation strategy, two case studies of simulations are carried out under different simulation conditions. The simulation environment is established using the high-fidelity CarSim-Simulink joint-simulation software platform, in which the CarSim software is used to provide the whole vehicle dynamic model, and the EDWM, the tire model, the WCKF-A, the WCKF-B, the tire force compensation module, and the longitudinal tire slip rate computation module, are established in Simulink software. The vehicle parameters are listed in Table 1.

TABLE 1. Vehicle parameters.

Symbol	Quantity	Value and units
m	vehicle mass	710 kg
r	effective radius of wheel	0.245 m
l_f	distances from vehicle gravity center to the front axle	0.795 m
lr	distances from vehicle gravity center to the rear axle	0.975 m
bf, br	half treads of the front(rear) wheels	0.775 m
C_f, C_r	equivalent cornering stiffness of front (rear) wheel	60000/40000 N/rad
I_z	moment of inertia	1000 kg·m^2
R	equivalent resistance of winding	0.688 Ω
K_a	inverse electromotive force coefficient	0.06 Nm/A
K_t	motor torque constant	11.43 Nm/A
J	sum of inertia moment of wheel and motor	7.143 kg·m^2
b	damping coefficient	0.643 Nm·sec/rad
L	equivalent inductance of winding	0.125H

$$\begin{bmatrix} x_{2,1,k} \\ x_{2,2,k} \\ x_{2,3,k} \end{bmatrix} = \begin{bmatrix} x_{2,1,k-1} + \left(x_{2,3,k-1}x_{2,2,k-1} + \frac{1}{m}\left(F_{x1,k-1} + F_{x2,k-1}\right)\cos\delta_{k-1} - \left(F_{y1,k-1} + F_{y2,k-1}\right)\sin\delta_{k-1} + F_{x3,k-1} + F_{x4,k-1}\right)\cdot T \\ x_{2,2,k-1} + \left(-x_{2,3,k-1}x_{2,1,k-1} + \frac{1}{m}\left(F_{x1,k-1} + F_{x2,k-1}\right)\sin\delta_k + \left(F_{y1,k-1} + F_{y2,k-1}\right)\cos\delta_{k-1} + F_{y3,k-1} + F_{y4,k-1}\right)\cdot T \\ \gamma_{k-1} + \frac{1}{I_z}\left[\left(F_{x1,k-1} + F_{x2,k-1}\right)l_f\sin\delta_{k-1} - \left(F_{y3,k-1} + F_{y4,k-1}\right)l_r + \left(F_{y1,k-1} + F_{y_{2,k-1}}\right)l_f\cos\delta_{k-1} \right. \\ \left. + \left(F_{y1,k-1} - F_{y2,k-1}\right)b_f\sin\delta_{k-1} - \left(F_{x1,k-1} - F_{x2,k-1}\right)b_f\cos\delta_{k-1} - \left(F_{x3,k-1} - F_{x4,k-1}\right)b_r\right]\cdot T \end{bmatrix} \tag{36}$$

A. CASE STUDY 1: SINUSOIDAL STEERING MANOEUVRE

In case study 1, the sinusoidal steering manoeuvre is carried out for the validation of designed estimation strategy, and the specific driving conditions of planned vehicle longitudinal speed and steering angle of hand wheel are shown in Fig. 4. It can be found that, during 0s to 6s, the vehicle longitudinal speed is 20m/s, then, the vehicle is accelerated evenly to 25m/s and then travels at a constant speed. In addition, the road friction coefficient is set to be 0.7. The comparisons of longitudinal force estimation results and longitudinal force compensation results are shown in Fig. 5, in which the TFC represent the longitudinal tire force compensation results, and the CarSim represent the actual longitudinal forces provided by the CarSim software. According to Fig. 5, we can see that the estimated results of WCKF-A and TFC are very close to the actual results of CarSim as a whole. Through the compensation of tire force, the estimation results of TFC have higher estimation accuracy. In the process of vehicle uniform motion, the estimated results are basically consistent with the actual results through tire force compensation. In the process of vehicle acceleration, the longitudinal force of vehicle increases sharply. Even in this case, the proposed estimation method can guarantee good tracking ability. Fig. 6 shows the estimation results of longitudinal vehicle speed, lateral vehicle speed, and vehicle sideslip angle by WCKF-A and WCKF-B. In the estimation results of longitudinal vehicle speed, it can be found that both WCKF-A and WCKF-B is competent for the estimation task. According to the partial enlarged drawing, one can see that the estimation effectiveness of WCKF-A is weaker than that of WCKF-B, which means that the presented estimation strategy can effectively suppress the estimation error and further improve the estimation accuracy. In the estimation results of lateral vehicle speed and vehicle sideslip angle, similarly, WCKF-B has more accurate estimation effect. It should be highlighted that, during about 11s to 13s, the estimation error of vehicle

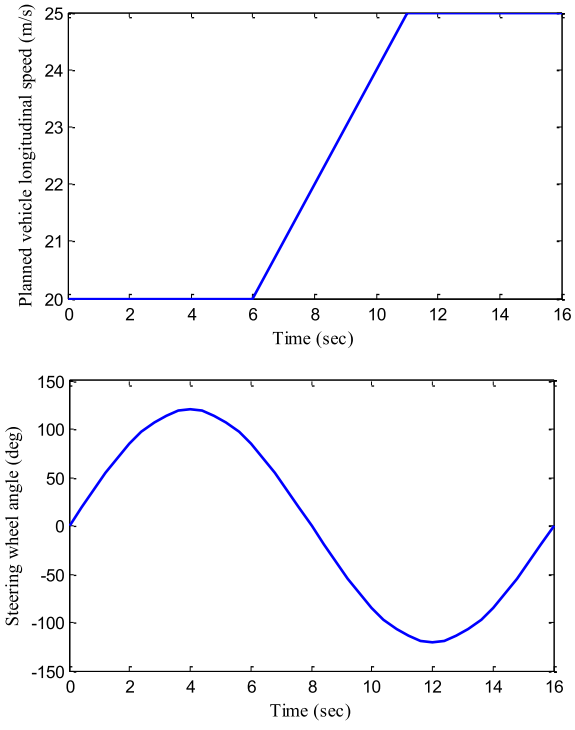

FIGURE 4. Sinusoidal steering manoeuvre.

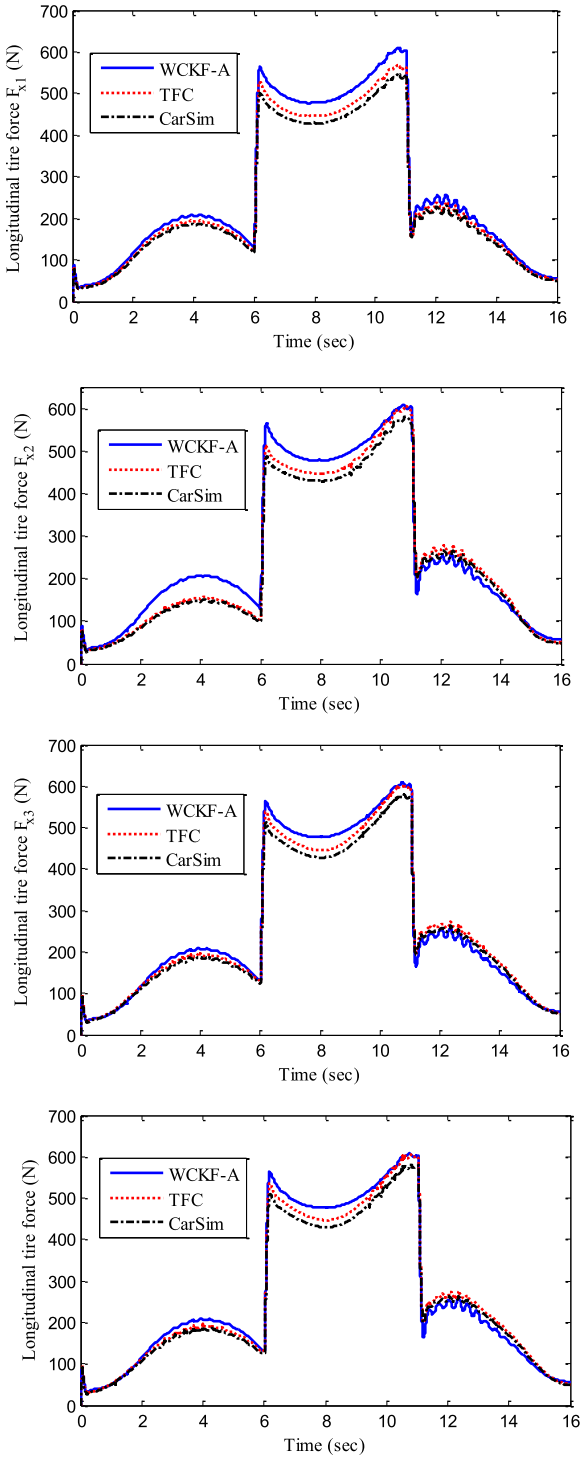

FIGURE 5. Estimation results of longitudinal forces in sinusoidal steering manoeuvre.

TABLE 2. Comparisons of pre in sinusoidal steering manoeuvre.

PRE	F_{x1}	F_{x2}	F_{x3}	F_{x4}	v_x	v_y	β
WCKF-A	4.3542	4.3312	4.2091	4.1247	0.1254	0.2017	N/A
TFC/WCKF-B	1.3669	1.2635	1.2785	1.2577	0.0469	0.0226	0.0357

sideslip angle is relatively large. This is because the longitudinal speed and steering wheel angle reach the maximum at this time, and the vehicle state changes dramatically, resulting in a slightly larger estimation error. However, it can be found that the proposed method still maintains good estimation performance.

In order to quantitatively testify the availability of the designed estimation strategy, the peak of relative error (PRE) and the error of root mean square (ERMS) between actual value and estimated value are used for contrast verification and can be obtained as

$$PRE(x) = x_{k/p} - x_{Carsim/p} \tag{37}$$

$$ERMS(x) = \sqrt{\frac{1}{N}\sum_{k=1}^{N}(x_k - x_{Carsim})^2} \tag{38}$$

where N represents the sample number, x_k represents the estimated vehicle states of WCKF-A, TFC, and WCKF-B at the kth sample, x_{CarSim} represents the actual vehicle states obtained by CarSim at the kth sample, $x_{k/p}$ represents the peak value of x_k, and $x_{CarSim/p}$ represents the peak value of x_{CarSim}. The comparison of PRE between WCKF-A and TFC about the estimation effect of longitudinal force and the comparison of PRE between WCKF-A and WCKF-B about the estimation effect of vehicle running states are listed in Table 2. The comparison of ERMS between WCKF-A and TFC and the comparison of PRE between WCKF-A and WCKF-B are listed in Table 3. In Table 2, we can see that the PRE of longitudinal force estimation results by WCKF-A is significantly larger than that of TFC, which indicates that the proposed compensation method reduces the estimation error of peak value. Similarly, the PRE of WCKF-A is larger than that of WCKF-B. In Table 3, the ERMS of WCKF-A is larger than that of TFC or WCKF-B, which indicates that the proposed method improves the estimation accuracy and stability as a whole.

B. CASE STUDY 2: J-TURN MANOEUVRE

In case study 2, the J-turn simulation manoeuvre is executed for further validation of presented estimation strategy in drastic steering conditions. In J-turn manoeuvre, the vehicle speed maintains at 15m/s, the road friction coefficient is set to be 1.0, and the steering angle of hand wheel is shown in Fig. 7. Fig. 8 shows the estimation results of longitudinal force in J-turn manoeuvre. At the moment of sudden turning, the longitudinal force of the vehicle has

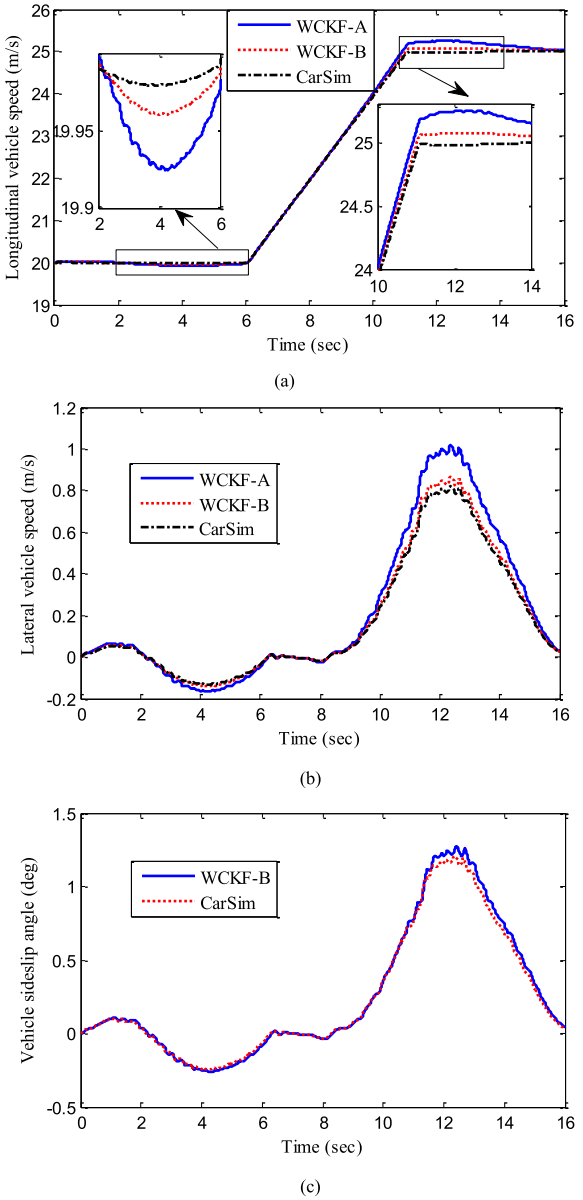

FIGURE 6. Estimation results of vehicle running states in sinusoidal steering manoeuvre. (a) Longitudinal vehicle speed. (b) Lateral vehicle speed. (c) Vehicle sideslip angle.

some jitter, but the jitter converges quickly, and the proposed method can also track the actual longitudinal force in real time. Then, as steering angle decreases, the accuracy of longitudinal force estimation increases correspondingly. Fig. 9 shows the estimation results of vehicle running states in

TABLE 3. Comparisons of erms in sinusoidal steering manoeuvre.

PRE	F_{x1}	F_{x2}	F_{x3}	F_{x4}	v_x	v_y	β
WCKF-A	0.3292	0.3132	0.3055	0.3092	0.2273	0.2384	N/A
TFC/WCKF-B	0.1164	0.1135	0.1098	0.1121	0.1008	0.0779	0.0863

TABLE 4. Comparisons of pre in j-turn manoeuvre.

PRE	F_{x1}	F_{x2}	F_{x3}	F_{x4}	v_x	v_y	β
WCKF-A	12.7893	12.5619	13.1221	12.9737	0.2583	0.0792	N/A
TFC/WCKF-B	2.8274	2.5504	2.9216	2.8756	0.1698	0.0223	0.0233

TABLE 5. Comparisons of erms in j-turn manoeuvre.

PRE	F_{x1}	F_{x2}	F_{x3}	F_{x4}	v_x	v_y	β
WCKF-A	0.8366	0.8214	0.8207	0.8091	0.1654	0.0541	N/A
TFC/WCKF-B	0.4582	0.4622	0.4479	0.4603	0.0825	0.0117	0.0164

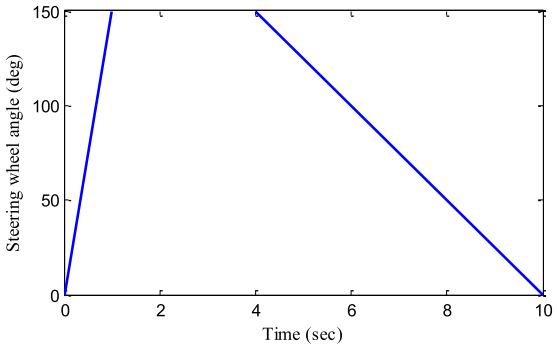

FIGURE 7. Steering wheel angle in J-turn manoeuvre.

J-turn manoeuvre. As shown in Fig. 9, same to case study 1, the estimation performance of designed strategy is also satisfactory. As shown in Table 4 and Table 5, according to the comparison results of PRE and ERMS, it can be summarized that the presented estimation strategy improves the performance of state estimation both in the overall estimation accuracy and in the error of a single data point, which illustrates that the presented estimation strategy can still maintain good estimation performance in severe vehicle steering process.

V. EXPERIMENTAL VERIFICATION

The road test is implemented for further experimental verification of proposed estimation strategy. The vehicle used for experimental verification is a four-wheel independent drive electric vehicle, which was refitted from a pure electric vehicle driven by a central motor. The rated power, maximum torque and maximum rotation speed of equipped in-wheel motor is 3KW, 150Nm and 750r/min, respectively. The electronic control system of the whole vehicle is built based on a rapid prototyping platform (RPP). The vehicle is equipped with high-precision differential global positioning system (GPS) and inertial navigation measuring unit (IMU), used for the measurements of vehicle trajectory and vehicle-body posture. The steering angle of front wheel is obtained by computing the measured hand steering wheel angle. Utilizing the CAN bus, the measurements of sensor signals of vehicle running states are recorded in host computer by the CAN tools of Vehicle SPY3. The electronic control system and sensor network of experimental vehicle are shown in Fig.10.

Under the current experimental conditions, the tire force sensor has not been installed on the test vehicle for direct measurement of longitudinal force. Therefore, the chassis dynamometer bench test is carried out before validating the effect of vehicle driving state estimation, and the experimental data are used to validate the longitudinal force estimation method. The principle of chassis dynamometer bench test is shown in Fig. 11. As shown in Fig. 11, the whole vehicle control is realized based on the RPP, and the running states of EDWM is collected by the CAN bus and used as the inputs of longitudinal force estimation. The chassis dynamometer data acquisition system is used to record the actual value of longitudinal force, which is compared with the estimated longitudinal force to verify the effectiveness of the proposed estimation method. The longitudinal force estimation result is shown in Fig. 12. It can be found that the estimated longitudinal force of WCKF-A has good estimation accuracy, although there are some chattering phenomena. The chattering phenomenon in the estimation results is due to the introduction

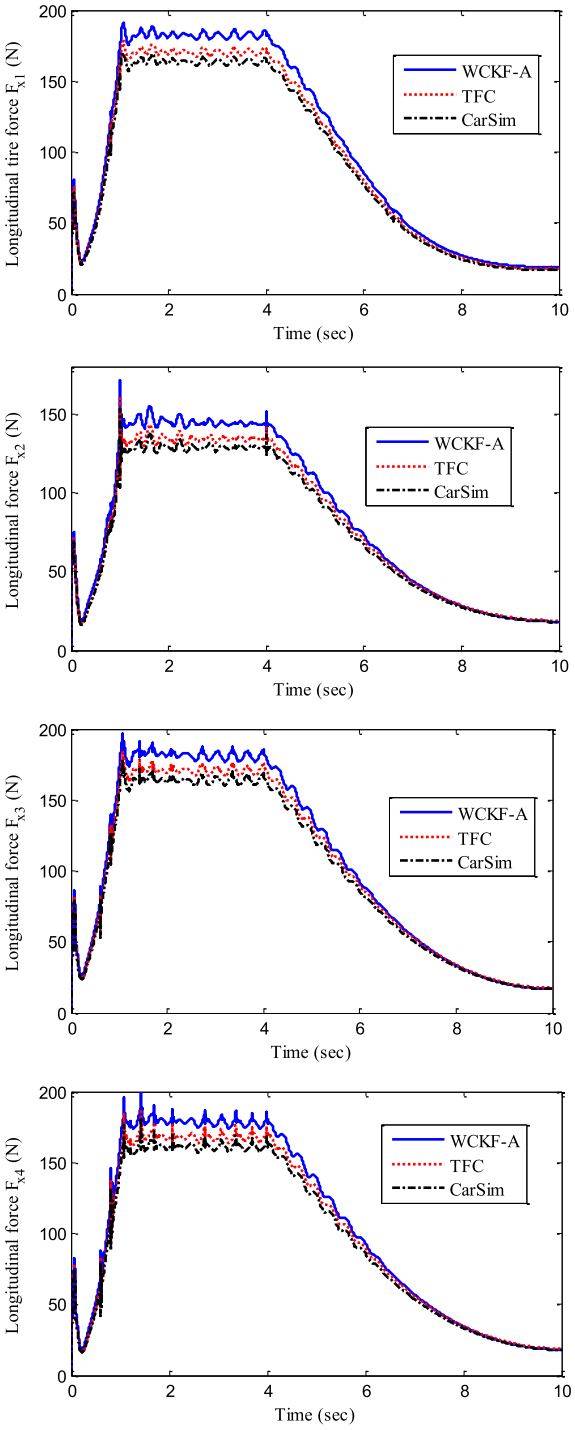

FIGURE 8. Estimation results of longitudinal forces in J-turn manoeuvre.

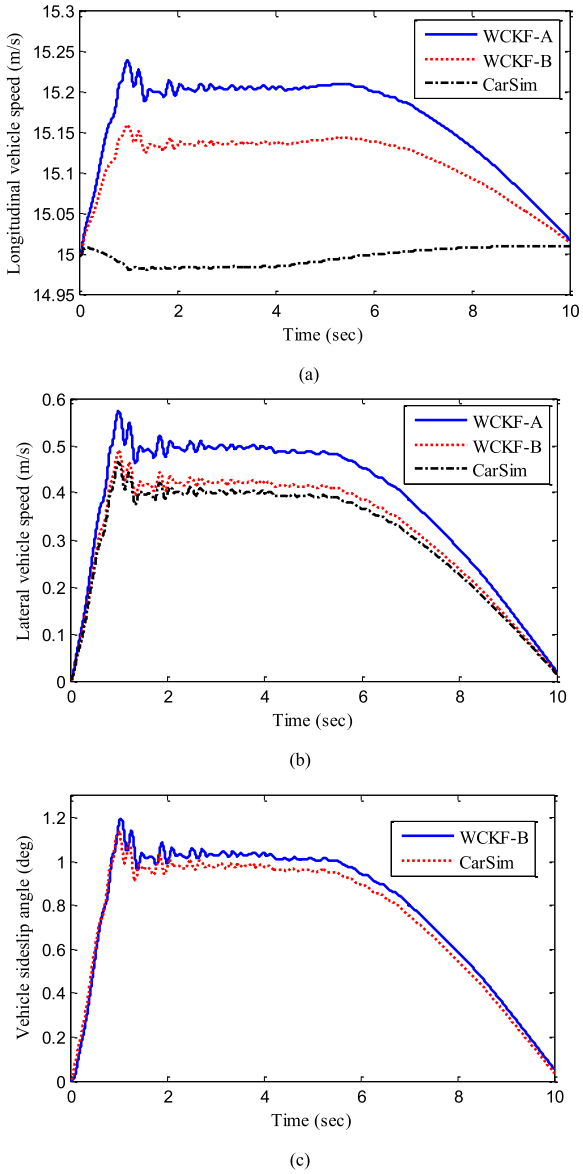

FIGURE 9. Estimation results of vehicle running states in sinusoidal steering manoeuvre. (a) Longitudinal vehicle speed. (b) Lateral vehicle speed. (c) Vehicle sideslip angle.

of a high-order sliding mode observer in the construction of the longitudinal force dynamic equation. The combination of high-order sliding mode observer and Kalman filter can effectively reduce the impact of chattering on estimation results. In addition, one can see that the estimation accuracy of longitudinal force has been further improved by means of longitudinal force compensation. With the longitudinal force estimation method been verified, in the state estimation verification of road test, the validated longitudinal force estimator is regarded as a reliable virtual sensor.

Fig. 13 shows the experimental vehicle, experimental environment, and the pictures of real sensor products in road test. As shown in Fig. 13, the serpentine road test was carried out, in which the 10 traffic piles are placed as the roadblock, and the vehicle speed cruising control is realized by a speed controller in RPP. The vehicle running states collected from the real vehicle test is shown in Fig. 14, and the verification results of proposed estimation strategy are shown in Fig. 15. It can be found that the proposed method can still maintain reliable and accurate estimation results in road test. In the

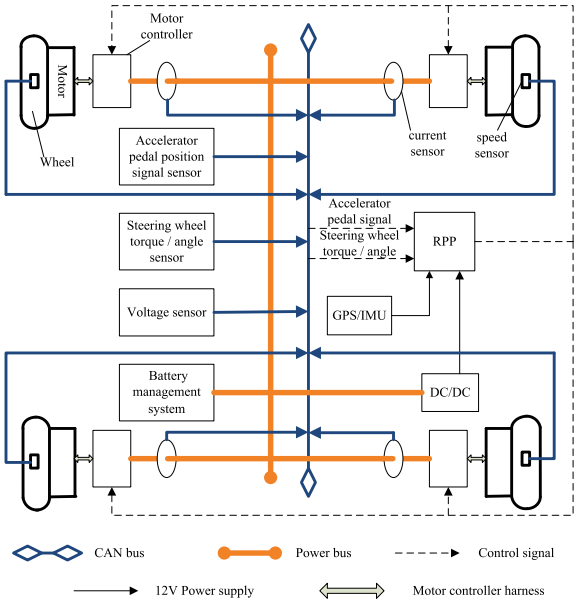

FIGURE 10. Control system and sensor network of experimental vehicle.

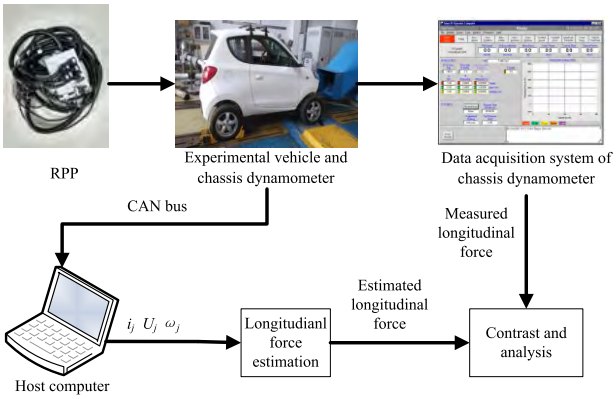

FIGURE 11. Chassis dynamometer bench test.

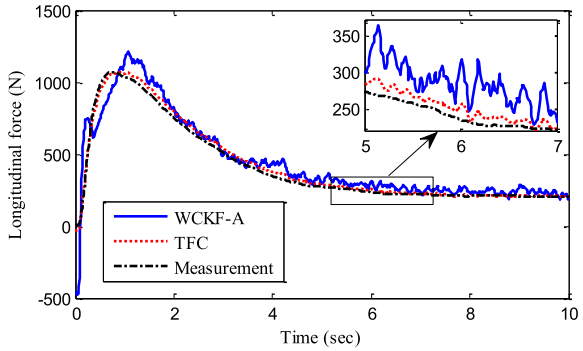

FIGURE 12. Longitudinal force estimation result in experiment.

TABLE 6. Comparisons of pre in experiment.

PRE	F_{xl}	v_x	v_y	β
WCKF-A	4.3542	0.1254	0.2017	N/A
TFC/WCKF-B	1.3669	0.0469	0.0226	0.0357

TABLE 7. Comparisons of erms in experiment.

PRE	F_{xl}	v_x	v_y	β
WCKF-A	0.3292	0.2273	0.2384	N/A
TFC/WCKF-B	0.1164	0.1008	0.0779	0.0863

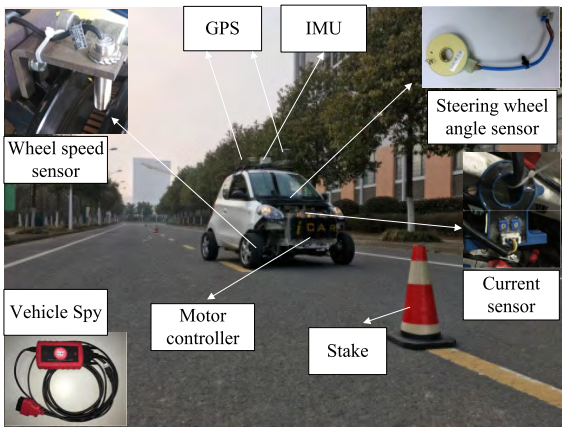

FIGURE 13. Road test.

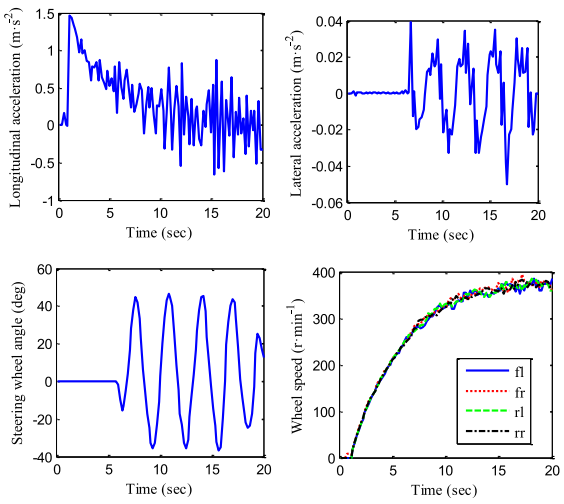

FIGURE 14. Vehicle running states in road test.

comparison of lateral vehicle speed and vehicle sideslip angle, the estimation error at the peak of state is relatively large. This is because the steering wheel angle of vehicle reaches the maximum at this time, and the vehicle driving state changes relatively quickly, so the requirement for the tracking ability of the filter is more stringent. In this case, the estimation performance of designed method is satisfactory. The comparison results of PRE and ERMS is shown in Table 6 and Table 7, respectively. Similarly, the PRE and ERMS of TFC and WCKF-B are evidently smaller than that

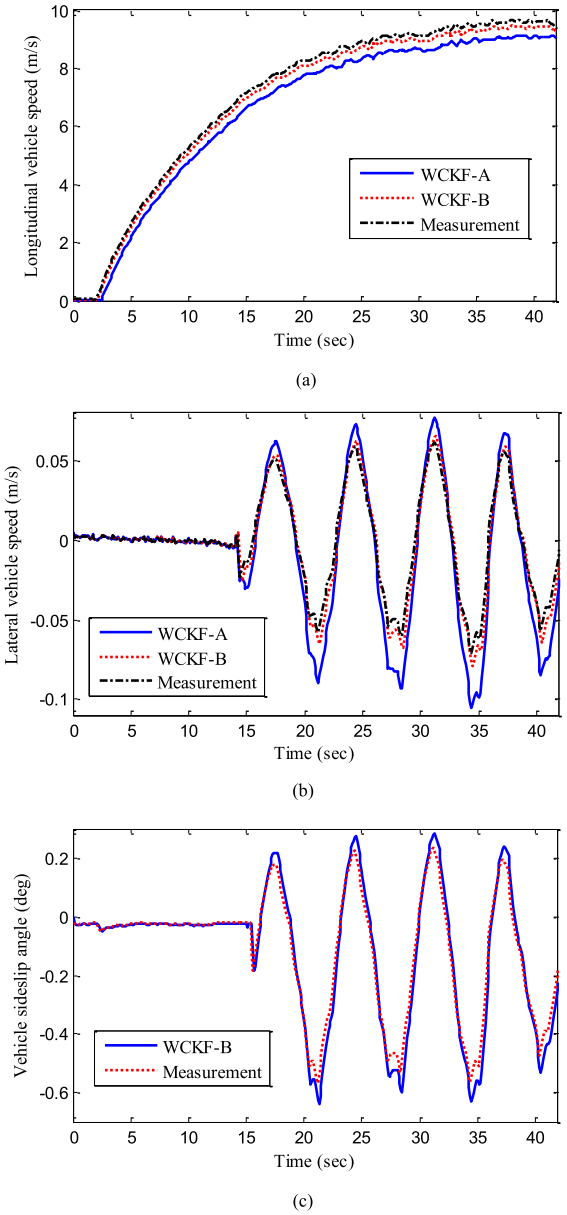

FIGURE 15. **Estimation results of vehicle running states in experiment. (a) Longitudinal vehicle speed, (b) Lateral vehicle speed, (c) Vehicle sideslip angle.**

of WCKF-A. Thus, the effectiveness of the proposed estimation strategy in practical application is verified.

VI. CONCLUSION

This paper presents a novel design of vehicle running states fused estimation strategy using the Kalman filters and tire force compensation method. In this paper, the 3-DOF vehicle dynamics model, EDWM, tire model and tire slip rate calculation model are established for the design of estimation method. Since the tire longitudinal force is the unknown input of EDWM, in order to promote the design of longitudinal force estimation method, a high-order sliding mode observer is introduced to construct the state space equation of the longitudinal force. Then, a weighted square-root cubature Kalman filter is studied and used for vehicle running states estimation, in which the covariance matrix of measurement noise is adjusted by using the moving window estimation method. According to the vehicle dynamics model and EDWM, the mode discretization is implemented, and then the preliminary estimation of vehicle driving state is obtained by using the above filtering algorithm. Using the preliminary estimation information, an overall estimation strategy with information fusion and tire force compensation is proposed, in which the tire force compensation method is designed to improve the accuracy and adaptability of tire force estimation, and the compensated tire force and the preliminary estimation information are re-used as the inputs of the new designed Kalman filter to improve the accuracy and reliability of the overall estimation strategy by using the fusion method of redundant information. The co-simulation in CarSim-Simulink model under multiple operating conditions and the real vehicle test are carried out. The simulation and experiment results verify the effectiveness of the proposed estimation strategy.

REFERENCES

[1] C. Hu, R. Wang, F. Yan, H. Huang, H. Wang, and C. Wei, "Differential steering based yaw stabilization using ISMC for independently actuated electric vehicles," *IEEE Trans. Intell. Transp. Syst.*, vol. 19, no. 2, pp. 628–638, Feb. 2018.

[2] A. Goodarzi and E. Esmailzadeh, "Design of a VDC system for all-wheel independent drive vehicles," *IEEE/ASME Trans. Mechatronics*, vol. 12, no. 6, pp. 632–639, Dec. 2007.

[3] R. Hou, L. Zhai, T. Sun, Y. Hou, and G. Hu, "Steering stability control of a four in-wheel motor drive electric vehicle on a road with varying adhesion coefficient," *IEEE Access*, to be published. doi: 10.1109/ACCESS.2019.2901058.

[4] R. Wang, C. Hu, Z. Wang, F. Yan, and N. Chen, "Integrated optimal dynamics control of 4WD4WS electric ground vehicle with tire-road frictional coefficient estimation," *Mech. Syst. Signal Process*, vols. 60–61, pp. 727–741, Aug. 2015.

[5] H. Zhang and J. Wang, "Active steering actuator fault detection for an automatically-steered electric ground vehicle," *IEEE Trans. Veh. Technol.*, vol. 66, no. 5, pp. 3685–3702, May 2017.

[6] T. Chen, L. Chen, X. Xu, Y. Cai, and X. Sun, "Simultaneous path following and lateral stability control of 4WD-4WS autonomous electric vehicles with actuator saturation," *Adv. Eng. Softw.*, vol. 128, pp. 46–54, Feb. 2019.

[7] H. Zhang, G. Zhang, and J. Wang, "H_∞ observer design for LPV systems with uncertain measurements on scheduling variables: Application to an electric ground vehicle," *IEEE/ASME Trans. Mechatronics*, vol. 21, no. 3, pp. 1659–1670, Jun. 2016.

[8] A. M. Dizqah, B. Lenzo, A. Sorniotti, P. Gruber, S. Fallah, and J. De Smet, "A fast and parametric torque distribution strategy for four-wheel-drive energy-efficient electric vehicles," *IEEE Trans. Ind. Electron.*, vol. 63, no. 7, pp. 4367–4376, Jul. 2016.

[9] L. Chen, T. Chen, X. Xu, Y. Cai, H. Jiang, and X. Sun, "Multi-objective coordination control strategy of distributed drive electric vehicle by orientated tire force distribution method," *IEEE Access*, vol. 6, pp. 69559–69574, Oct. 2018.

[10] H. Jiang, A. Li, S. Ma, and L. Chen, "Design and performance analysis of airflow energy recovery device of electric vehicle," *J. Jiangsu Univ., Natural Sci. Ed.*, vol. 38, no. 2, pp. 125–132, Apr. 2017.

[11] H. Zheng, J. Zhou, Q. Shao, and Y. Wang, "Investigation of a longitudinal and lateral lane-changing motion planning model for intelligent vehicles in dynamical driving environments," *IEEE Access*, vol. 7, pp. 44783–44802, 2019. doi: 10.1109/ACCESS.2019.2909273.

[12] J. H. Guo, Y. G. Luo, and K. Q. Li, "Integrated adaptive dynamic surface car-following control for nonholonomic autonomous electric vehicles," *Sci. China Technol. Sci.*, vol. 8, pp. 1221–1230, Aug. 2017.

[13] Y. Cai, Z. Liu, H. Wang, and X. Sun, "Saliency-based pedestrian detection in far infrared images," *IEEE Access*, vol. 5, pp. 5013–5019, 2017.
[14] H. Qiu, Z. Dong, and Z. Lei, "Simulation and experiment of integration control of ARS and DYC for electrical vehicle with four wheel independent drive," *J. Jiangsu Univ., Natural Sci. Ed.*, vol. 37, no. 3, pp. 268–276, Jun. 2016.
[15] Y. Wang, H. Fujimoto, and S. Hara, "Torque distribution-based range extension control system for longitudinal motion of electric vehicles by LTI modeling with generalized frequency variable," *IEEE/ASME Trans. Mechatronics*, vol. 21, no. 1, pp. 443–452, Feb. 2016.
[16] T. Goggia, A. Sorniotti, L. de Novellis, A. Ferrara, P. Gruber, J. Theunissen, D. Steenbeke, B. Knauder, and J. Zehetner, "Integral sliding mode for the torque-vectoring control of fully electric vehicles: Theoretical design and experimental assessment," *IEEE Trans. Veh. Technol.*, vol. 64, no. 5, pp. 1701–1715, May 2015.
[17] H. Guo, H. Chen, D. Cao, and W. Jin, "Design of a reduced-order nonlinear observer for vehicle velocities estimation," *IET Control Theory Appl.*, vol. 7, no. 17, pp. 2056–2068, Nov. 2013.
[18] H. Guo, H. Chen, F. Xu, F. Wang, and G. Lu, "Implementation of EKF for vehicle velocities estimation on FPGA," *IEEE Trans. Ind. Electron.*, vol. 60, no. 9, pp. 3823–3835, Sep. 2013.
[19] G. De Filippis, B. Lenzo, A. Sorniotti, P. Gruber, and W. De Nijs, "Energy-efficient torque-vectoring control of electric vehicles with multiple drivetrains," *IEEE Trans. Veh. Technol.*, vol. 67, no. 6, pp. 4702–4715, Jun. 2018. doi: 10.1109/TVT.2018.2808186.
[20] Z. Li, W. Wang, X. Xu, and K. Jiang, "Willans model of electric motor for electric vehicle based on least squares support vector machine," *J. Jiangsu Univ., Natural Sci. Ed.*, vol. 37, no. 4, pp. 381–385, Aug. 2016.
[21] T. Chen, X. Xu, Y. Li, W. Wang, and L. Chen, "Speed-dependent coordinated control of differential and assisted steering for in-wheel motor driven electric vehicles," *Proc. Inst. Mech. Eng. D, J, Automobile Eng.*, vol. 232, no. 9, pp. 1206–1220, Aug. 2018.
[22] B. L. Boada, M. L. Boada, and V. Diaz, "Vehicle sideslip angle measurement based on sensor data fusion using an integrated ANFIS and an unscented Kalman filter algorithm," *Mech. Syst. Signal Process*, vol. 72, pp. 832–845, May 2016.
[23] T. Chen, L. Chen, X. Xu, Y. Cai, H. Jiang, and X. Sun, "Estimation of longitudinal force and sideslip angle for intelligent four-wheel independent drive electric vehicles by observer iteration and information fusion," *Sensors*, vol. 18, no. 4, p. 1268, Apr. 2018.
[24] T. Chen, L. Chen, Y. Cai, and X. Xu, "Estimation of vehicle sideslip angle via pseudo-multisensor information fusion method," *Metrol. Meas. Syst.*, vol. 25, no. 3, pp. 499–516, Sep. 2018.
[25] W. Liu, H. He, and F. Sun, "Vehicle state estimation based on minimum model error criterion combining with extended Kalman filter," *J. Franklin Inst.*, vol. 353, pp. 834–856, Mar. 2016.
[26] Y.-H. Liu, T. Li, Y.-Y. Yang, X.-W. Ji, and J. Wu, "Estimation of tire-road friction coefficient based on combined APF-IEKF and iteration algorithm," *Mech. Syst. Signal Process*, vol. 88, pp. 25–35, May 2017.
[27] T. Chen, X. Xu, L. Chen, H. Jiang, Y. Cai, and Y. Li, "Estimation of longitudinal force, lateral vehicle speed and yaw rate for four-wheel independent driven electric vehicles," *Mech. Syst. Signal Process.*, vol. 101, pp. 377–388, Feb. 2018.
[28] X. Xu, T. Chen, L. Chen, and W. Wang, "Longitudinal force estimation for motorized wheels driving electric vehicle based on improved closed-loop subspace identification," *J. Jiangsu Univ., Natural Sci. Ed.*, vol. 37, no. 6, pp. 650–656, Dec. 2016.
[29] G. Morrison and D. Cebon, "Sideslip estimation for articulated heavy vehicles at the limits of adhesion," *Vehicle Syst. Dyn.*, vol. 54, no. 11, pp. 1601–1628, Nov. 2016.
[30] M. Doumiati, A. C. Victorino, A. Charara, and D. Lechner, "Onboard real-time estimation of vehicle lateral tire–road forces and sideslip angle," *IEEE/ASME Trans. Mechatronics*, vol. 16, no. 4, pp. 601–614, Aug. 2011.
[31] K. Nam, Y. Hori, and C. Lee, "Wheel slip control for improving traction-ability and energy efficiency of a personal electric vehicle," *Energies*, vol. 8, no. 7, pp. 6820–6840, 2015.
[32] K. Nam, H. Fujimoto, and Y. Hori, "Lateral stability control of in-wheel-motor-driven electric vehicles based on sideslip angle estimation using lateral tire force sensors," *IEEE Trans. Veh. Technol.*, vol. 61, no. 5, pp. 1972–1985, Jun. 2012.
[33] W. Li, X. Zhu, and J. Ju, "Hierarchical braking torque control of in-wheel-motor-driven electric vehicles over CAN," *IEEE Access*, vol. 6, pp. 65189–65198, 2018. doi: 10.1109/ACCESS.2018.2877960.
[34] B. Shyrokau, D. Wang, D. Savitski, K. Hoepping, and V. Ivanov, "Vehicle motion control with subsystem prioritization," *Mechatronics*, vol. 30, pp. 297–315, Sep. 2015.
[35] X. Zhang and D. Göhlich, "Integrated traction control strategy for distributed drive electric vehicles with improvement of economy and longitudinal driving stability," *Energies*, vol. 10, no. 1, p. 126, Jan. 2017.
[36] G. Baffet, A. Charara, and D. Lechner, "Estimation of vehicle sideslip, tire force and wheel cornering stiffness," *Control Eng. Pract.*, vol. 17, no. 11, pp. 1255–1264, 2009.
[37] L. Li, J. Song, H. Li, Z. Xiaolong, L. Li, and X. Zhang, "A variable structure adaptive extended Kalman filter for vehicle slip angle estimation," *Int. J. Veh. Des.*, vol. 56, nos. 1–4, pp. 161–185, Oct. 2011.
[38] K. T. Leung, J. F. Whildborne, D. Purdy, and A. Dunoyer, "A review of ground vehicle dynamic state estimations utilising GPS/INS," *Vehicle Syst. Dyn.*, vol. 49, nos. 1–2, pp. 29–58, Feb. 2011.
[39] L. Li, G. Jia, X. Ran, J. Song, and K. Wu, "A variable structure extended Kalman filter for vehicle sideslip angle estimation on a low friction road," *Veh. Syst. Dyn.*, vol. 52, no. 2, pp. 280–308, Jan. 2014.
[40] X. Li, X. Song, and C. Chan, "Reliable vehicle sideslip angle fusion estimation using low-cost sensors," *Measurement*, vol. 51, pp. 241–258, May 2014.
[41] X. Li, C.-Y. Chan, and Y. Wang, "A reliable fusion methodology for simultaneous estimation of vehicle sideslip and yaw angles," *IEEE Trans. Veh. Technol.*, vol. 65, no. 6, pp. 4440–4458, Jun. 2016.
[42] K. Nam, S. Oh, H. Fujimoto, and Y. Hori, "Estimation of sideslip and roll angles of electric vehicles using lateral tire force sensors through RLS and Kalman filter approaches," *IEEE Trans. Ind. Electron.*, vol. 60, no. 3, pp. 988–1000, Mar. 2013.
[43] X. Jin and G. Yin, "Estimation of lateral tire–road forces and sideslip angle for electric vehicles using interacting multiple model filter approach," *J. Franklin Inst.*, vol. 352, pp. 686–707, Feb. 2015.
[44] D. Pi, N. Chen, J. X. Wang, and B. J. Zhang, "Design and evaluation of sideslip angle observer for vehicle stability control," *Int. J. Automot. Technol.*, vol. 12, no. 3, pp. 391–399, Jun. 2011.
[45] D. M. Bevly, J. Ryu, and J. C. Gerdes, "Integrating INS sensors with GPS measurements for continuous estimation of vehicle sideslip, roll, and tire cornering stiffness," *IEEE Trans. Intell. Transp. Syst.*, vol. 7, no. 4, pp. 483–493, Dec. 2006.
[46] H. Zhang, X. Huang, J. Wang, and H. RezaKarimi, "Robust energy-to-peak sideslip angle estimation with applications to ground vehicles," *Mechatronics*, vol. 30, pp. 338–347, Sep. 2015.
[47] B. Zhang, H. Du, J. Lam, N. Zhang, and W. Li, "A novel observer design for simultaneous estimation of vehicle steering angle and sideslip angle," *IEEE Trans. Ind. Electron.*, vol. 63, no. 7, pp. 4357–4365, Jul. 2016.
[48] T. Chen, L. Chen, Y. Cai, and X. Xu, "Robust sideslip angle observer with regional stability constraint for an uncertain singular intelligent vehicle system," *IET Control Theory Appl.*, vol. 12, no. 13, pp. 1802–1811, Sep. 2018.
[49] K. T. Leung, J. F. Whidborne, D. Purdy, and P. Barber, "Road vehicle state estimation using low-cost GPS/INS," *Mech. Syst. Signal Process*, vol. 25, no. 6, pp. 1988–2004, Aug. 2011.
[50] J.-H. Yoon and H. Peng, "Robust vehicle sideslip angle estimation through a disturbance rejection filter that integrates a magnetometer with GPS," *IEEE Trans. Intell. Transp. Syst.*, vol. 15, no. 1, pp. 191–204, Feb. 2014.
[51] J.-H. Yoon and H. Peng, "A cost-effective sideslip estimation method using velocity measurements from two GPS receivers," *IEEE Trans. Veh. Technol.*, vol. 63, no. 6, pp. 2589–2599, Jul. 2014.
[52] J.-H. Yoon, S. E. Li, and C. Ahn, "Estimation of vehicle sideslip angle and tire-road friction coefficient based on magnetometer with GPS," *Int. J. Automot. Technol.*, vol. 17, no. 3, pp. 427–435, Jun. 2016.
[53] A. K. Madhusudhanan, M. Corno, and E. Holweg, "Vehicle sideslip estimator using load sensing bearings," *Control Eng. Pract.*, vol. 54, pp. 46–57, Sep. 2016.

TE CHEN was born in Henan, China, in 1992. He received the B.S. degree in mechanical design, manufacturing, and automation from the North China University of Water Resources and Electric Power, Zhengzhou, China, in 2014, and the M.S. degree in automotive engineering from Jiangsu University, Zhenjiang, in 2017, where he is currently pursuing the Ph.D. degree in automotive engineering.

His current research interests include state estimation and the dynamics control of vehicles.

YINGFENG CAI was born in Jiangsu, China, in 1985. She received the B.S., M.S., and Ph.D. degrees from the School of Instrument Science and Engineering, Southeast University, Nanjing, China. In 2013, she joined the Automotive Engineering Research Institute, Jiangsu University, as an Assistant Professor.

Her research interests include computer vision, intelligent transportation systems, and intelligent automobiles.

LONG CHEN was born in Jiangsu, China, in 1958. He received the B.S. and Ph.D. degrees in mechanical engineering from Jiangsu University, Zhenjiang, China, in 1982 and 2006, respectively, where he is currently a Professor with the Automotive Engineering Research Institute.

His research interests include electric vehicles, electric drives, the simulation and the control of vehicle dynamic performance, vehicle operation, and transport planning.

XING XU was born in Jiangsu, China, in 1979. He received the B.S. degree in vehicle engineering, the M.S. degree in control theory and control engineering, and the Ph.D. degree in agricultural electrification and automation from Jiangsu University, Zhenjiang, China, in 2002, 2006, and 2010, respectively, where he is currently a Professor and a Doctoral Supervisor of the Automotive Engineering Research Institute.

His research interests include the modeling, identification, optimization, fault diagnosis, and the control of vehicle dynamic systems.

HAOBIN JIANG was born in Jiangsu, China, in 1969. He received the B.S. degree in agricultural mechanization from Nanjing Agricultural University, Nanjing, China, in 1991, and the M.S. and Ph.D. degrees in vehicle engineering from Jiangsu University, Zhenjiang, China, in 1994 and 2000, respectively.

His research interests include vehicle dynamic performance analysis and electrical control technology.

XIAOQIANG SUN was born in 1989. He received the Ph.D. degree from Jiangsu University, China, in 2016. He is currently a Lecturer with the Automotive Engineering Research Institute, Jiangsu University.